Geothermics 104 (2022) 102442

Contents lists available at ScienceDirect

Geothermics

journal homepage: www.elsevier.com/locate/geothermics

Transient assessment of an earth air heat exchanger in warm climatic conditions

Yousef Belloufi [a,b,*], Sakina Zerouali [c], Amar Rouag [d,e], Faris Aissaoui [f,b], Rachid Atmani [b], Abdelhafid Brima [b], Noureddine Moummi [b]

[a] Université Kasdi Merbah Ouargla, Faculté des Hydrocarbures, des Energies Renouvelables, des Sciences de la Terre et de l'Univers, Département de Forage et Mécanique des Chantiers Pétroliers, BP 511 Ouargla 30000, Algeria
[b] Laboratoire de Génie Mécanique (LGM), Université Mohamed Khider Biskra, BP 145 Biskra 07000, Algeria
[c] Université Mostefa Ben Boulaïd Batna 2, Faculté de Technologie, Département de Socle Commun Science et Technique, BP 05078 Fesdis-Batna, Algeria
[d] Université Kasdi Merbah Ouargla, Faculté des Hydrocarbures, des Energies Renouvelables, des Sciences de la Terre et de l'Univers, Département des Energies Renouvelables, BP 511 Ouargla 30000, Algeria
[e] Laboratoire de Génie Energétique et Matériaux (LGEM), Université Mohamed Khider Biskra, BP 145 Biskra 07000, Algeria
[f] Université de Ghardaïa, Faculté des sciences et de la technologie, Département d'Automatique et Electromécanique, Ghardaïa 47000, Algeria

ARTICLE INFO

Keywords:
Earth air heat exchanger
Transient thermal performance
Continuous operation
Derating factor
Summer cooling

ABSTRACT

The Earth Air Heat Exchanger (EAHE) is a promising passive technique that utilises shallow geothermal energy to improve the thermal comfort in buildings. EAHE has the potential to minimize the amount of electrical energy used by traditional air conditioning systems. The aim of this research is to examine the thermal performance of the EAHE under continuous operation. A transient numerical model was developed using the implicit finite difference method. Afterwards, the thermal performance was evaluated by using the means of derating factor. In addition, an experimental setup is realised in Biskra University (Algeria) to take measurements during cooling period. According to numerical calculations, the high thermal performance of EAHE is dependant on high thermal conductivity of soil and low air velocity. The values of the derating factor in the studied cases ranged from 0% to 35% that can mislead the design of the EAHE if ignored. The experimental findings revealed that for 3.5 m/s of air velocity, the maximum air temperature drop can reach up 19 °C. It is noticed that the initial 33 m of the pipe can provide 91% of the whole reduction in air temperature. In extreme real cases, the maximum air temperature increasing does not exceed 0.85 °C during all 95 h. Consequently, ambient temperature decreases during night operation and then cools the heated subsoil and assists the soil to recover its cooling capacity.

1. Introduction

In recent decades, the world has suffered from the very high consumption of electrical energy required for air conditioning. This high consumption is clearly appear in the Saharan areas, especially during the cooling period. To meet these energy challenges, several cooling techniques using alterative energies can be implemented. EAHEs are part of geothermal energy that refers heat energy stored in the subsoil, where the energy coming from the subsoil is mainly consumed in form of heat.

(Liu et al., 2019a; Liu et al., 2019b) proposed and designed a vertical EAHE based on a buried vertical U-tube. The main advantages of the vertical EAHE compared to the horizontal EAHE lie in its deeper pipe depths (more than 15 m). This allow soil temperatures to stabilize at the needed source temperature, as well as the fact that it requires less land occupation (less than 1 m^2) and therefore making it suitable for usage in densely build regions (Zhou et al., 2016; Xi et al., 2017). Furthermore, the vertical EAHE has a higher geothermal energy use efficiency and a simpler discharge of air condensate water to avoid the growth of bacteria, which will improve the air supply quality (Liu et al., 2019c; Liu et al., 2021). In addition, the vertical EAHE plays a very important role to enhance heat transfer efficiency and therefore improve the EAHE's thermal performance (Bozis et al., 2011; Jalaluddin et al. 2011). On the other hand, amongst the drawbacks of vertical EAHE is that their layout necessitates a significant amount of drilling depth, which increases the expense of a geothermal ventilation system. Horizontal EAHE could be employed if there are open regions (Zhelykh et al., 2016). Śliwa et al. (2018) discussed other disadvantages of the vertical EAHE such as: the need for a drilling rig with elevators, a high lifting capacity and implementation of centralizers, which must ensure that the two pipes

* Corresponding author.
E-mail address: yousef_belloufi@yahoo.fr (Y. Belloufi).

https://doi.org/10.1016/j.geothermics.2022.102442
Received 7 February 2022; Received in revised form 1 May 2022; Accepted 4 May 2022
Available online 8 May 2022

Nomenclature

C_p	Specific heat [J/Kg. °C]
h	Convective heat transfer coefficient [W/m^2. °C]
m	Mass [Kg]
R	Thermal Resistance [°C/W]
R_i	Thermal resistance per unit length [°C /W.m]
r_1	Pipe inner radius [m]
r_2	Pipe outer radius [m]
r_3	Undisturbed soil radius [m]
s	Surface [m]
t	Time [s]
T_1	Air temperature at the pipe inlet [°C]
T_a	Flowing air temperature [°C]
T_i	Undisturbed soil temperature [°C]
T_{soil}	Soil temperature [°C]
u	Air flow velocity [m/s]

Greek symbols

α	Soil thermal diffusivity [m^2/s]
λ_{soil}	Soil thermal conductivity [W/m. °C]
ρ	Air density [kg/m^3]
EAHE	Earth air heat exchanger

are stable inside the borehole. All these factors affect also the maintenance cost comparing to horizontal EAHE, which is intended for cooling and ventilation buildings.

Several researchers have studied horizontal EAHE systems, to evaluate and enhance its thermal behaviour, whether using theoretical modelling or by experiments. Mihalakakou (2003) used a dynamic and deterministic model to predict the EAHE's heating potential. He validated experimentally the estimated values of soil temperature, the author concluded that the air temperature at the outlet of EAHE could be efficiently simulated by the neural network and it affected by the soil temperature. (Benhammou and Draoui 2015; Cuny et al., 2019; Minaei et al., 2021) observed that heat transfer decreases by increasing pipe length and the increase the mass flow rate causes saturation of soil. Lee and Strand (2008) presented the heating and cooling potential in buildings using an EAHE, they concluded that no remarkable benefits in using EAHE more than 70 m of length. According to Ahmed et al. (2016) EAHE length parameter dominates other thermo-physics parameters of the system (pipe material, air velocity and soil conductivity) that affect the EAHE thermal performances. Niu et al. (2015) tested five air velocities (0.5, 1.0, 2 and 2.5 m/s) in cooling mode, they found that low flow velocity of 0.5 m/s provides more time to evacuate its heat to nearer soil to the EAHE and thus a high temperature drop.

Rodrigues et al. (2015) presented a numerical study to enhance the thermal performance of an EAHE by using the Constructal Design Method. It was found that the increasing of buried pipes number and keeping same air mass flow rate could enhance the thermal performance of EAHE up to 73% and 115% for cooling and heating respectively. Kumar et al. (2003) studied numerically EAHE with 80 m of tube length. They concluded that the used system could create 296 kWh heating potential and 456 kWh cooling potential and can keep the room temperature at 27.65 °C. Misra et al. (2013b) used CFD analysis and derating factor to evaluate EAHE system according to the following parameters: soil thermal conductivity, pipe length, inlet air velocity and operation duration. The results showed that high air velocity and poor soil conductivity affect the EAHE's thermal behaviour. Barakat et al. (2016) presented a numerical study to evaluate the thermal performance of EAHE. The system that is assembled to gas turbine is used to enhance the power performance. The results reveal that there is an increase in both output power and efficiency with values of 4.8% and 9% respectively.

Rouag et al. (2018) developed a new semi analytical method called 'RBM' to design EAHE system. The calculation algorithm is based on the Bessel functions to estimate the soil temperature. The authors have fixed the heat flux at the inner pipe diameter for the full time step. The results showed that the soil radius can reach 55 cm at constant inlet air temperature condition in the case of 6 h of operation. Mehdid et al. (2018) used the RBM model proposed by Rouag et al. (2018) to predict the air temperature under transient conditions. Moreover, an experimental measurement is used to validate the developed model 'GRBM'. The authors summarized that this model can be used as practical tool to design EAHE system. Belloufi et al. (2017) investigated the EAHE's transient thermal behaviour in summer cooling in continuous operation mode. They validated the numerical results with measured air temperatures on site of Biskra University, Algeria. Due to high soil conductivity, the continuous operation of 71 h had no discernible influence on the outlet air temperature. Menhoudj et al. (2018) investigated the influence of pipe material on EAHE's thermal performance in cooling mode in Algeria. Results showed that the decrease in air temperature can reach 6.5 °C for zinc pipe and 6 °C for PVC pipe. Therefore, the authors noted that the pipe material is not considered in the evaluating of thermal performance of EAHE. At this regards, a lot of parameters including pipe material are analysed by Rosa et al. (2018). They also noticed that the type of pipe have no effect on the performance of the system due to very low increase in COP. However, the most important factor is the air velocity. Hamdane et al. (2021) presented a theoretical approach to calculate the outlet air temperature. The authors used finite difference method to estimate the axial air temperature and the two dimensional soil temperature in steady and transient conditions respectively. They concluded that in comparison to prior models, the model is less sensitive to the operation duration as well as the periodic temperature condition at the EAHE's inlet.

Hermes et al. (2020) analysed the thermal behaviour of three different EAHEs installations located in Rio Brande, Brazil. They used finite volume computational model in the simulation. From the results, it noticed that 2 m depth is considered an ideal pipe placement depth and can increase the EAHE thermal potential in cooling and heating periods. In intermittent and continuous operation modes, Mathur et al. (2015b) compared the soil self-recovery ability and thermal saturation. To develop the EAHE model, the authors used a three-dimensional simulation software package, ANSYS 14.5. They concluded that soil temperature can recovered more in the continuous mode than intermittent if the nighttime ambient air temperature is significantly lower than the soil temperature. Mathur et al. (2015a) examined the EAHE's thermal performance in transient conditions. Three intermittent operation modes are considered for three soil thermal conductivity. Three dimensional transient numerical model was applied in the CFD analysis. It noticed that EAHE with higher soil conductivity can be run continuously while EAHE with poor soil conductivity can be used in intermittent mode. Fazlikhani et al. (2017) developed a theoretical steady state model to assess the effect of various factors on the heating and cooling potential of EAHE in cold (Hamadan) and hot-arid (Yazd) climates respectively. In the winter, the potential for rising air temperature in Hamadan and Yazd was found to be in the range of 0.1 - 17 °C and 0.2 - 11.2 °C respectively. On the other hand in cooling period, the air temperature decreases of 5.7 to 11.1 °C and 1.3 to 11.4 °C respectively. They concluded that, geothermal EAHE have the ability to take up the role of cooler in arid and hot climate.

Zajch and Gough (2021) relies on a climate-based approach and 492 weather files to compare the heating and cooling potential in Canada for different seasonal variation scenarios. They investigate EAHE's seasonal sensitivity to changes in air or soil temperatures caused by natural changes in soil surface energy partitioning. Yang and Zhang (2015) proposed an analytical solution for evaluating the thermal performance of EAHE under periodic fluctuations in both soil and inlet ambient air temperatures. The authors found that the coupling of EAHE with

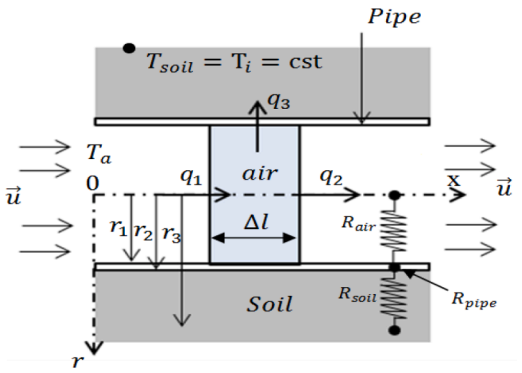

Fig. 1. One-dimensional scheme of the EAHE.

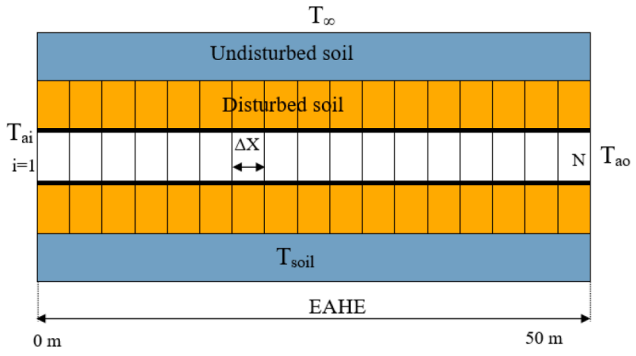

Fig. 2. Discretized domain of the EAHE.

building can maintain a building's thermal comfort. (Yang et al., 2016; Wei and Yang 2019) developed mathematical models for analysing the heat transfer in flat rectangular and circular EAHEs under harmonic fluctuations, and they compared the differences in thermal performances. It was showed that the outlet air temperature fluctuation of the flat rectangular EAHE was lower, and the wall temperature of EAHE pipe was more stable compared to the circular EAHE. An experimental study carried out by (Wei et al., 2020; Wei et al., 2021) of an EAHE integrated to a building to provide space cooling and heating. It was shown that the EAHE can be used as a pre-conditioning system to heat air in cold climates and to cool air in hot regions. On the other hand, the EAHE system has been found to be highly effective in diverse climates.

Through the literature review above, it's clear that duration operation and thermo-physical properties have an important influence on the functioning of EAHE system. Furthermore, not much literature is available on the concept of soil thermal saturation and EAHE's self-recovery, which is an important factor that determines the useful EAHE's operation duration. On the other hand, few researches studied experimentally and theoretically in detailed manner the effect of these parameters on the performance of EAHE to achieve an optimum design as function of time.

At this regards, the main objective of this work is to suggest both experimental and numerical analyses to predict the EAHE's thermal performances during extreme summer conditions. The influence of soil properties, air velocity and continuous functioning were analysed. The parameter called Derating Factor 'DF' using the temperature decrease under steady and transient conditions is determined. An experimental setup was realized at the University of Biskra (Algeria) to examine the effect of continuous operation mode on thermal performance in hot and arid climatic conditions. Besides, the self-recovery capacity of the soil is investigated to predict the thermal deterioration with time. For this reasons, the experimental measurements were conducted during the summer period from July to September 2013.

2. Mathematical models

The following assumptions have been considered to simplify the thermal calculation (Belloufi 2017; Mehdid et al., 2018):

- Thermo-physical properties of air and soil are constant.
- Along the buried pipe, the convective heat transfer coefficient is constant.
- Soil moisture is neglected.
- From a distance δ of the buried pipe surface, the soil temperature remains constant.
- Longitudinal conduction is neglected.

2.1. Modelling the eahe system

The transient one-dimensional soil temperature is governed by the following Fourier's equation:

$$\frac{\partial^2 T_{soil}}{\partial z^2} = \frac{1}{\alpha}\frac{\partial T_{soil}}{\partial t} \tag{1}$$

Considering the following initial and boundary conditions:

$$\begin{aligned} &T_{soil}(z=0,t) = T_i + A\cos[w(t-t_0)] \\ &T_{soil}(z\to\infty,t) = T_i \\ &T_{soil}(z,t=0) = T_i \end{aligned} \tag{2}$$

Where T_{soil} is the soil temperature, α is the soil thermal diffusivity, T_i is the undisturbed soil temperature, A is the soil temperature amplitude and $w = 2\pi/365$ [rad/day] is the angular frequency.

The solution of this problem yields the following equation for calculating soil temperature (Belloufi 2017):

$$T_{soil}(z,t) = T_i + Aexp\left(-\sqrt{\frac{w}{2\alpha}}z\right)\cos\left[w(t-t_0) - \sqrt{\frac{w}{2\alpha}}z\right] \tag{3}$$

Then, transient one-dimensional energy balance equation has been adopted to calculate outlet air temperature as shown in Fig. 1.

The heat transfer between the soil and the air inside the pipe can be expressed as follows:

$$mc_{pair}\frac{DT_a}{Dt} = q_1 - q_2 - q_3 \tag{4}$$

From Eq. (4), it can obtain:

$$mc_{pair}\left(\frac{\partial T_a}{\partial t} + u\frac{\partial T_a}{\partial x}\right) = -\lambda_{air}\, s\frac{\partial T_a}{\partial x}\Big|_l + \lambda_{air}\, s\frac{\partial T_a}{\partial x}\Big|_{l+\Delta l} + \frac{(T_{soil} - T_a)}{R_{total}} \tag{5}$$

Where the total thermal resistance is denoted by the symbol R_{total}:

$$R_{total} = R_{soil} + R_{pipe} + R_{cv} \tag{6}$$

Where:

$R_{soil} = \frac{1}{2\pi.\ \lambda_{soil}.\ \Delta l} ln(r_3(t)/r_2)$ is the soil thermal resistance;

$R_{pipe} = \frac{1}{2\pi.\ \lambda_{pipe}.\ \Delta l} ln(r_2/r_1)$ is the pipe thermal resistance;

$R_{cv} = \frac{1}{2\pi\ h\ r_1\ \Delta l}$ is the convective thermal resistance;

$h = (Nu\ k)/(2\ r_1)$ is the heat transfer coefficient by convection inside the pipe;

$N_u = 0.023 R_e^{0.8} P_r^{0.3}$ is the Nusselt number (Al-Ajmi et al., 2006; de Jesus Freire et al. 2013; Barakat et al., 2016);

$R_e = \rho u/\mu$ is the Reynolds number (Al-Ajmi et al., 2006);

$r_3(t) = \sqrt{\alpha.t/\pi}$ is the distance between the external pipe surface and undisturbed soil (Hollmuller 2003).

Eq. (5) reduced by taking into account that longitudinal conduction and heat transfer by convection are neglected.

$$\rho s c_{pair}\left(\frac{\partial T_a}{\partial t} + u\frac{\partial T_a}{\partial x}\right) = \frac{(T_{soil} - T_a)}{R_{itotal}} \tag{7}$$

Fig. 3. Experimental setup of EAHE.

Fig. 4. Detailed placement of the air temperature sensor in the EAHE.

Fig. 5. Data acquisition unit.

Table 1
Characteristic of measuring equipment.

Equipment	Range of measuring	Precision	Resolution
Propeller anemometer	0.3 - 35 m/s	3.1 – 35 m/s 0.3 – 3 m/s	0.1 m/s 0.01 m/s
Temperature detector 'RTD'	−50 to 200 °C		10^{-5} °C

R_{itotal} is the thermal resistance divided by unit length (Δl).

$$\frac{\partial T_a}{\partial t} = -u\frac{\partial T_a}{\partial x} + \frac{(T_{soil} - T_a)}{\gamma} \tag{8}$$

With $\gamma = \rho\, \pi\, r_1^2\, c_{pair}\, R_{itotal}$

Choosing the following boundary conditions in order to solve Eq. (8).

$T_a\ (x = 0) = T_1$

Table 2
Physical and thermal properties used in the proposed model.

Physical and thermal parameters	Values
Air density (kg/m^3)	1.2
Air flow velocity (m/s)	3.5
Internal diameter of the pipe (m)	0.1
Pipe thermal conductivity (W/m. °C)	0.17
Soil thermal conductivity (W/m. °C)	1.25
Specific heat capacity of air (J/Kg. °C)	1000
Undisturbed soil temperature (°C)	26

$T_a\ (t = 0) = T_{soil}$ (Philippe et al., 2009; Mnasri and Younès 2010; Diersch et al., 2011).

To solve Eq. (8), both the time and space domains represented in Fig. 2 are discretized using implicit finite differences method. In the discretization, the centred finite differences method is used up to node N-1 and the left finite differences method is employed to calculate the final node.

If the index 'i' denotes the variable 'x' and the index 'k' denotes the variable 't', the implicit finite differences equation will be getting by writing the second member of Eq. (8) at next time $(k + 1)$ where the solution is not known, which gives (Nougier 1987):

$$\frac{1}{\Delta t}\left(T_{i,k+1} - T_{i,k}\right) = -\frac{u}{2\Delta x}\left(T_{i+1,k+1} - T_{i-1,k+1}\right) - \frac{1}{\gamma}T_{i,k+1} + \frac{T_{soil}}{\gamma} \tag{9}$$

$\Delta t = L/u$ represents the required time for a slice of air to travel the entire length of the pipe.

After rearrangement, it obtain:

$$T_{i,k} + \frac{\Delta t}{\gamma}T_{soil} = -\frac{u\ \Delta t}{2\Delta x}T_{i-1,k+1} + \left(\frac{\Delta t}{\gamma} + 1\right)T_{i,k+1} + \frac{u\ \Delta t}{2\Delta x}T_{i+1,k+1} \tag{10}$$

This discretized equation is designed for a mesh going from the second node to the node N-1

For the last node N (outlet air temperature), the left finite differences is applied to Eq. (8) as follows:

$$\frac{1}{\Delta t}\left(T_{N,k+1} - T_{N,k}\right) = -\frac{u}{\Delta x}\left(T_{N,k+1} - T_{N-1,k+1}\right) - \frac{1}{\gamma}T_{N,\ k+1} + \frac{T_{soil}}{\gamma} \tag{11}$$

Therefore, the equation giving the air temperature in the final node N is written as follows:

$$T_{N,k} + \frac{\Delta t}{\gamma}T_{soil} = -\frac{u\ \Delta t}{\Delta x}T_{N-1,k+1} + \left(\frac{u\ \Delta t}{\Delta x} + \frac{\Delta t}{\gamma} + 1\right)T_{N,\ k+1} \tag{12}$$

Eqs. (10) and (12) were solved by the developed program and Thomas method is applied to calculate the transient temperature of the air along the EAHE.

2.2. Derating factor

To calculate the derating factor DF in thermal performance, the temperature difference in steady state between inlet and outlet of the pipe is considered as reference for evaluating EAHE's thermal performance in transient condition. The derating factor DF is calculated using the air temperatures decrease obtained in both transient and steady state conditions (Bansal et al., 2013; Benhammou and Draoui 2015).

$$DF = \frac{(T_{inlet} - T_{outlet})_{transient\ state}}{(T_{inlet} - T_{outlet})_{steady\ state}} \tag{13}$$

Where:

T_{outlet} in transient state is derived from Eq. (10).

T_{outlet} in steady state is derived from the solution of Eq. (8) in steady state as follows (Belloufi 2017).

$$\rho\pi\ r_1^2\ c_{pair}\ u\frac{dT_a}{dx} = \frac{(T_{soil} - T_a)}{R_{itotal}} \tag{14}$$

Table 3
Experimental air temperature variation inside the EAHE on days of (23–25 July 2013).

Duration of operation (h : m)	Air temperatures inside the EAHE (°C), $u = 2$ m/s. Length of pipe (m)														
	Inlet	3.63	7.69	11.73	16.04	20.07	24.12	26.37	29.07	33.10	37.01	38.86	40.82	45.10	48.80
09:30 (After 1 h)	39.37	38.00	34.77	32.49	31.30	30.42	29.41	29.18	28.90	28.47	27.97	27.77	27.60	27.23	27.11
13:30	44.15	41.19	36.76	33.62	32.23	31.06	29.84	29.53	29.16	28.67	28.09	27.88	27.70	27.27	27.14
17:30	45.53	42.92	38.07	34.64	33.02	31.64	30.25	29.88	29.43	28.89	28.24	28.01	27.81	27.34	27.21
21:30	39.64	37.97	35.24	33.17	31.96	30.99	29.90	29.63	29.28	28.79	28.20	27.98	27.80	27.34	27.22
01:30	36.53	35.57	33.68	32.18	31.21	30.47	29.57	29.36	29.09	28.66	28.13	27.92	27.75	27.33	27.21
05:30	31.98	32.27	31.56	30.95	30.28	29.83	29.18	29.05	28.87	28.50	28.04	27.85	27.69	27.32	27.19
09:30	36.90	36.30	33.88	32.07	31.08	30.35	29.46	29.26	29.02	28.61	28.11	27.91	27.74	27.35	27.22
13:30	42.78	40.28	36.27	33.46	32.14	31.06	29.92	29.63	29.28	28.80	28.22	28.01	27.82	27.39	27.26
17:30	44.03	41.77	37.52	34.40	32.91	31.66	30.33	29.98	29.56	29.02	28.37	28.13	27.94	27.44	27.31
21:30	39.03	37.45	34.97	33.02	31.90	31.00	29.96	29.70	29.38	28.90	28.31	28.09	27.91	27.44	27.31
01:30	36.27	35.36	33.59	32.19	31.25	30.54	29.66	29.46	29.20	28.77	28.23	28.03	27.85	27.42	27.30
05:30	32.62	32.72	31.93	31.16	30.52	30.05	29.37	29.23	29.05	28.66	28.18	27.99	27.82	27.42	27.29
08:30 (After 48 h)	36.40	35.84	33.71	32.01	31.14	30.45	29.59	29.40	29.16	28.74	28.24	28.03	27.86	27.45	27.32

Table 4
Experimental air temperature variation inside the EAHE on days of (04–07 August 2013).

Duration of operation (h :m)	Air temperatures inside the EAHE (°C), $u = 3.5$ m/s. Length of pipe (m)														
	Inlet	3.63	7.69	11.73	16.04	20.07	24.12	26.37	29.07	33.10	37.01	38.86	40.82	45.10	48.80
09:30 (After 1 h)	34.83	34.75	32.92	31.28	30.71	30.16	29.47	29.37	29.24	28.89	28.46	28.28	28.13	27.81	27.69
13:30	40.63	39.16	36.23	33.77	32.76	31.79	30.67	30.40	30.09	29.58	28.98	28.75	28.56	28.07	27.94
17:30	42.62	41.14	37.75	34.96	33.75	32.60	31.30	30.94	30.55	29.97	29.28	29.02	28.80	28.22	28.08
21:30	37.34	36.52	34.86	33.41	32.57	31.85	30.89	30.65	30.37	29.87	29.26	29.02	28.82	28.27	28.13
01:30	34.25	33.95	33.00	32.16	31.59	31.12	30.42	30.27	30.09	29.67	29.15	28.94	28.76	28.27	28.13
05:30	32.13	32.26	31.79	31.38	30.94	30.64	30.09	30.00	29.89	29.53	29.07	28.87	28.71	28.27	28.13
09:30	36.56	36.33	34.49	32.91	32.20	31.55	30.68	30.48	30.25	29.80	29.25	29.03	28.84	28.34	28.20
13:30	42.56	40.60	37.27	34.57	33.52	32.48	31.28	30.96	30.61	30.06	29.40	29.15	28.95	28.37	28.23
17:30	42.80	41.36	38.11	35.42	34.22	33.08	31.78	31.39	30.98	30.37	29.63	29.36	29.13	28.48	28.33
21:30	37.30	36.61	35.12	33.76	32.96	32.25	31.30	31.05	30.77	30.23	29.59	29.35	29.13	28.52	28.37
01:30	33.60	33.54	32.91	32.31	31.79	31.38	30.71	30.57	30.40	29.97	29.43	29.21	29.03	28.50	28.35
05:30	29.71	30.45	30.71	30.88	30.59	30.46	30.07	30.04	29.97	29.66	29.22	29.03	28.87	28.44	28.28
09:30	38.50	37.97	35.66	33.62	32.92	32.15	31.17	30.92	30.66	30.16	29.55	29.32	29.12	28.55	28.40
13:30	45.03	42.62	38.86	35.84	34.56	33.33	31.97	31.58	31.16	30.53	29.77	29.50	29.27	28.61	28.45
17:30	47.29	44.52	39.85	36.28	34.82	33.41	31.95	31.53	31.06	30.42	29.64	29.37	29.14	28.49	28.34
21:30	37.79	37.03	35.44	34.11	33.14	32.36	31.37	31.12	30.81	30.27	29.60	29.35	29.13	28.53	28.38
01:30	34.92	34.68	33.72	32.86	32.19	31.64	30.88	30.71	30.50	30.04	29.45	29.22	29.03	28.48	28.33
05:30	34.31	34.01	33.14	32.36	31.79	31.34	30.65	30.52	30.34	29.92	29.37	29.15	28.97	28.46	28.31
08:30 (After 72 h)	37.87	37.32	35.43	33.76	33.03	32.30	31.35	31.11	30.85	30.35	29.72	29.48	29.28	28.67	28.52

After integrating Eq. (14), it can obtain:

$$ln(T_a - T_{soil}) = -\left(\frac{1}{\rho\ \pi\ r_1^2\ c_{pair}\ u\ R_{itotal}}\right)x + C \quad (15)$$

Where C is an integration constant, it can obtained by applying a constant temperature at the EAHE's inlet.

The outlet air temperature can be expressed as follows:

$$T_a(x) = T_{soil} + (T_1 - T_i)\ exp\left[-\frac{1}{\rho\ \pi\ r_1{}^2 c_{pair}\ u\ R_{itotale}}x\right] \quad (16)$$

To evaluate the heat accumulation rejected on the soil, it is recommended to calculate the soil temperature at the first layer of undisturbed soil using Eq. (16) with injecting Ta (x) from experimental measurements as following:

$$T_{soil} = T_a(x) - (T_1 - T_i)\ exp\left[-\frac{1}{\rho\ \pi\ r_1{}^2 c_{pair}\ u\ R_{itotale}}x\right] \quad (17)$$

3. Experimental setup

This work was carried out in the LGM laboratory, University of Biskra. The EAHE shown in Fig. 3 composed of a PVC pipe divided into four horizontal parts of 48 m total length and 0.1 m diameter, buried at a depth of 3 m, which was previously determined based on local site data, with a slope of 2% and spacing of 2 m. To drain the condensed water, a sink is built right at the EAHE's outlet. Fig. 5 shows a data acquisition unit supplied by National Instrument (NI) coupled to 15 temperature detectors of the RTD type (Resistance Temperature Detector) along the EAHE. The air flow velocity is managed by an extractor with variable flow and reliable consumption in electrical energy (120 W) and measured by an propeller anemometer at the EAHE's outlet. The temperatures of air inside the pipe were measured at different distances along the EAHE. Air temperature detectors are correctly placed in the EAHE as shown in Fig. 4. In continuous operation during the cooling period, air temperatures along the pipe were taken every 15 min. Tables 1 and 2 show the instruments technical characteristics and the EAHE's main parameters.

4. Results

Tables 3, 4 and 5 illustrate the hourly air temperature variation for 15 sections inside the EAHE. As well as the impact of EAHE's continuous operation on its thermal performances. It is noted that temperatures of the air up to length of 33 m presented in Tables 3, 4 and 5 are unstable over time due to the effect of changing temperature at the pipe's inlet. In addition, the high temperatures induce heat build-up on the pipe's nearby soil. The ambient air temperatures drops at night, cooling the heated soil nearby the EAHE and assisting the soil in regaining its ability

Table 5
Experimental air temperature variation inside the EAHE on days of (18–19 September 2013).

Duration of operation (h :m)	Air temperatures inside the EAHE (°C), u = 4.5 m/s. Length of pipe (m)														
	Inlet	3.63	7.69	11.73	16.04	20.07	24.12	26.37	29.07	33.10	37.01	38.86	40.82	45.10	48.80
10:30 (After 1 h)	35.37	34.99	33.60	32.39	31.89	31.47	30.91	30.85	30.77	30.45	30.06	29.88	29.72	29.40	29.27
12:30	38.09	37.52	35.56	33.84	33.16	32.51	31.69	31.51	31.32	30.90	30.41	30.20	30.02	29.58	29.44
16:30	40.80	39.72	37.41	35.31	34.56	33.72	32.66	32.37	32.08	31.53	30.92	30.68	30.47	29.85	29.70
20:30	35.75	35.22	34.30	33.56	33.02	32.60	31.95	31.82	31.67	31.26	30.77	30.56	30.38	29.85	29.71
00:30	33.64	33.42	32.92	32.53	32.18	31.95	31.48	31.42	31.35	31.02	30.62	30.42	30.27	29.82	29.68
04:30	30.72	30.96	31.05	31.25	31.07	31.08	30.84	30.88	30.91	30.68	30.38	30.22	30.08	29.75	29.60
08:30	34.88	34.76	33.59	32.59	32.24	31.91	31.36	31.28	31.20	30.88	30.50	30.31	30.16	29.77	29.62
12:30	41.70	40.44	37.81	35.52	34.75	33.88	32.82	32.52	32.23	31.69	31.08	30.84	30.64	30.00	29.86
16:30	41.27	39.94	37.81	35.87	35.11	34.29	33.21	32.91	32.60	32.02	31.36	31.10	30.89	30.17	29.98
20:30	38.11	37.18	35.83	34.69	34.05	33.50	32.68	32.48	32.27	31.78	31.21	30.96	30.77	30.13	29.98
00:30	35.85	35.35	34.50	33.81	33.32	32.94	32.30	32.16	32.01	31.59	31.09	30.87	30.69	30.11	29.96
04:30	34.78	34.40	33.73	33.21	32.79	32.51	31.96	31.87	31.77	31.40	30.96	30.75	30.58	30.07	29.91
08:30	32.73	33.37	32.81	32.42	32.05	31.88	31.46	31.42	31.38	31.09	30.72	30.53	30.39	29.97	29.83
12:30	39.26	38.60	36.65	34.86	34.23	33.55	32.64	32.41	32.19	31.70	31.14	30.90	30.71	30.12	29.96
16:30	40.35	39.44	37.57	35.83	35.06	34.27	33.26	32.97	32.67	32.10	31.46	31.21	30.99	30.27	30.12
20:30	36.93	36.27	35.22	34.30	33.79	33.33	32.61	32.44	32.26	31.81	31.27	31.03	30.85	30.22	30.07
00:30	33.52	33.46	33.14	32.91	32.57	32.38	31.93	31.87	31.79	31.45	31.02	30.82	30.66	30.14	29.99
04:30	29.92	30.46	30.88	31.48	31.17	31.26	31.09	31.15	31.20	30.99	30.69	30.52	30.39	30.02	29.89
08:30	30.11	30.61	30.79	31.09	30.87	30.95	30.79	30.86	30.93	30.67	30.49	30.34	30.21	29.91	29.77
12:30	35.52	35.49	34.30	33.24	32.78	32.40	31.79	31.69	31.59	31.24	30.82	30.63	30.47	30.02	29.87
16:30	37.17	36.88	35.47	34.13	33.60	33.10	32.35	32.18	32.01	31.58	31.08	30.87	30.69	30.14	29.98
20:30	23.99	26.08	28.08	30.18	29.95	30.38	30.56	30.74	30.89	30.68	30.55	30.41	30.29	29.98	29.85
00:30	26.18	27.11	28.11	29.14	29.22	29.63	29.81	30.00	30.22	30.18	30.08	29.96	29.88	29.74	29.61
04:30	24.79	25.89	27.08	28.33	28.52	29.02	29.31	29.56	29.83	29.82	29.81	29.73	29.65	29.61	29.46
08:30 (After 95 h)	27.46	28.39	28.77	29.21	29.28	29.56	29.63	29.80	29.98	29.92	29.86	29.75	29.66	29.59	29.47

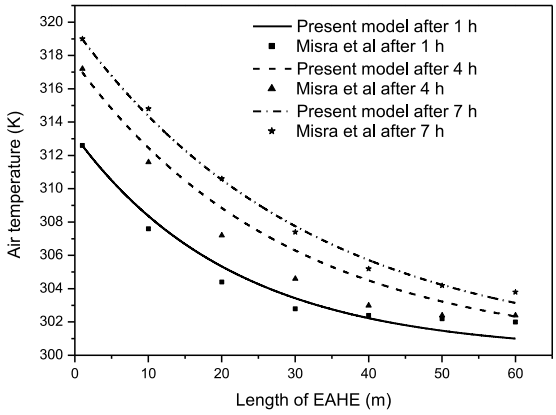

Fig. 6. Validation of the suggested model using experimental measurements of Misra et al. (2013a).

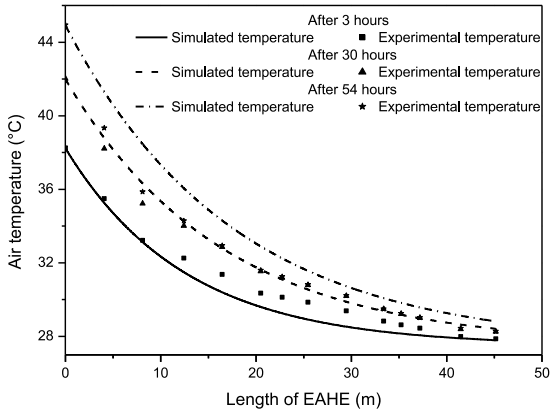

Fig. 7. Validation of the suggested model using self-experimental measurements.

Table 6
Main parameters used for comparative validation with Misra et al. (2013a).

Parameter	Value
Air flow velocity	5 m/s
Pipe diameter	0.1 m
Pipe length	60 m
Pipe thermal conductivity	1.16 W/m.k
Soil thermal conductivity	0.52 W/m.k
Undisturbed soil temperature (°C)	27

to cool. The air temperatures presented in outlet of the EAHE are almost constant and no noticeable effect is recorded of heat accumulation on thermal performance in the outlet of EAHE, due to the soil temperature self recovers at night operation. It is stated that first 33 m of the pipe can provide 89% of the total air temperature drop. From Tables 3, 4 and 5, the greatest increase in air temperature at the EAHE exit has been noticed to be 0.85 °C. Besides, it can be concluded that EAHE's thermal

Table 7
Numerical air temperature drop at the pipe's exit.

Pipe's length (m)	Air temperature inside the EAHE (°C)					
	(T_{inlet} - T_{outlet}) in steady state	(T_{inlet} - T_{outlet}) in transient conditions				
		1h	3h	6 h	12h	24h
Inlet	0	0	0	0	0	0
5	3.69	4.69	4.18	3.89	3.62	3.38
10	10.29	10.07	9.1	8.54	8.03	7.56
15	14.80	14.09	12.91	12.22	11.57	10.97
20	17.87	17.09	15.86	15.12	14.42	13.75
25	19.98	19.34	18.15	17.41	16.7	16.02
30	21.41	21.02	19.92	19.22	18.53	17.87
35	22.39	22.28	21.29	20.65	20.01	19.37
40	23.06	23.21	22.35	21.77	21.19	20.6
45	23.52	23.92	23.17	22.66	22.14	21.6

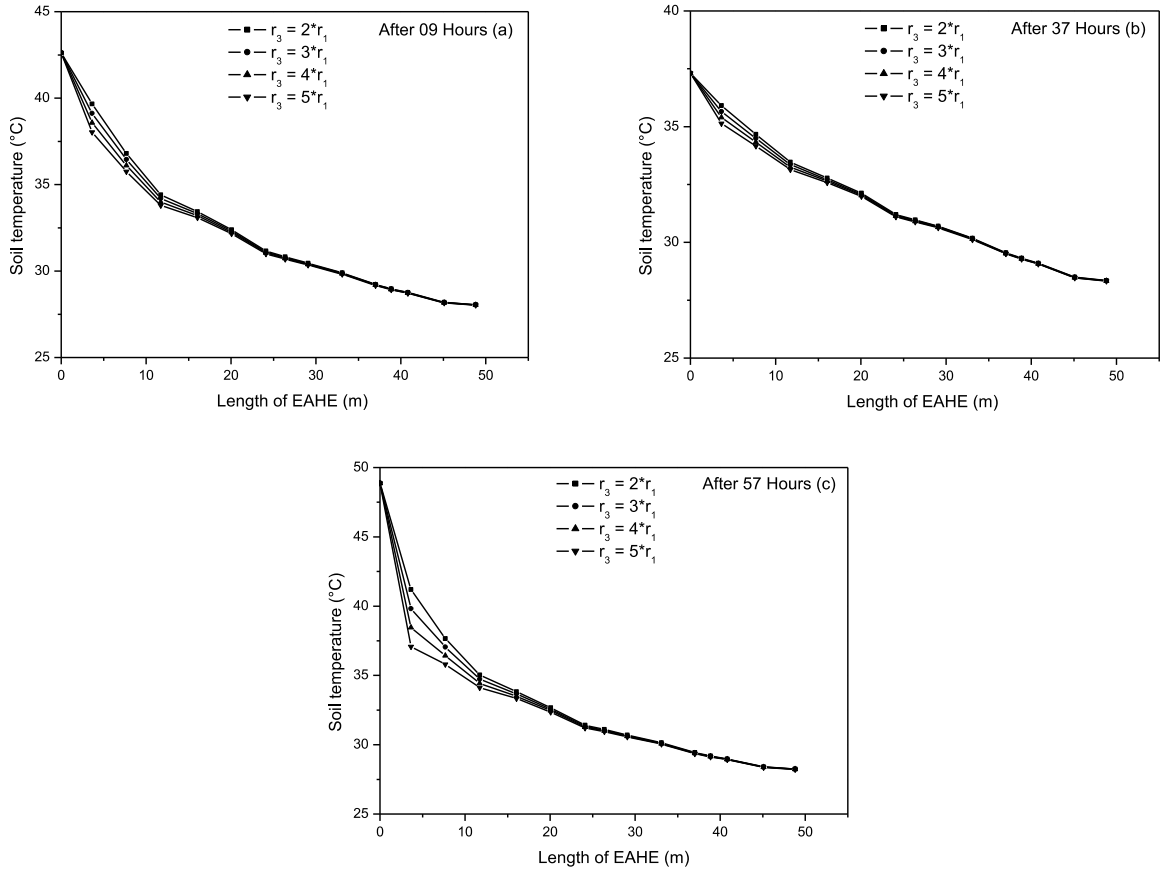

Fig. 8. Hourly soil temperature variation in different rays of the soil along the EAHE.

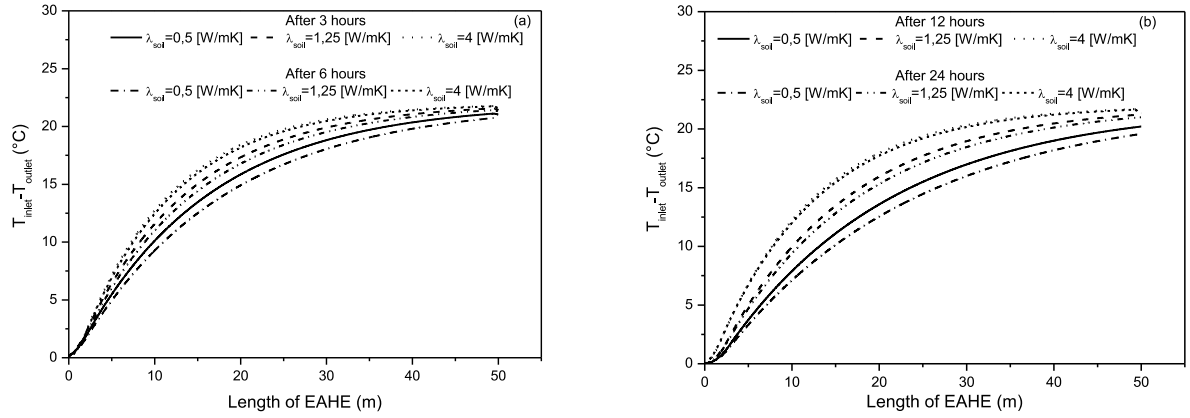

Fig. 9. Transient air temperature drop inside the EAHE for various soil thermal conductivities.

performance is unaffected by the continuous operating mode.

The experimental values of Misra et al. (2013a) were used to validate the developed transient numerical model (Fig. 6) for cooling cycle in Ajmer, India. Table 6 presents the main parameters used in the validation.

It can be seen in Fig. 6a good agreement between the simulated results and those of the experimental, mean relative errors of 1.98, 2.99 and 0.87 are obtained after 1 h, 4 h and 7 h respectively during the functioning of EAHE. Therefore, the developed model is validated and can be used for further analysis.

Moreover, the comparison to experimental data of other researchers, the previous section's model was also validated with self-experimental results that was carried out at the site of Biskra University. The days from 04 to 07 August 2013 (table 4) are chosen as typical days to perform this validation. From the analysis of validation results shown in Fig. 7, mean relative errors of 1.86, 0.47 and 2.40% are recorded after 1 h, 30 h and 54 h respectively during the functioning of the EAHE in continuous operation mode. The comparisons between computed values and self-experimental data show satisfactory agreement, which validates the developed numerical study.

To clearly show the impact of different parameters on the EAHE's thermal performance, the derating factor is used assuming a constant temperature at the pipe's inlet during the EAHE's operation. A maximum inlet air temperature can be used to simulate the effect of various parameters on the thermal performance of EAHE. The derating factor 'DF' is determined using the temperature differences obtained

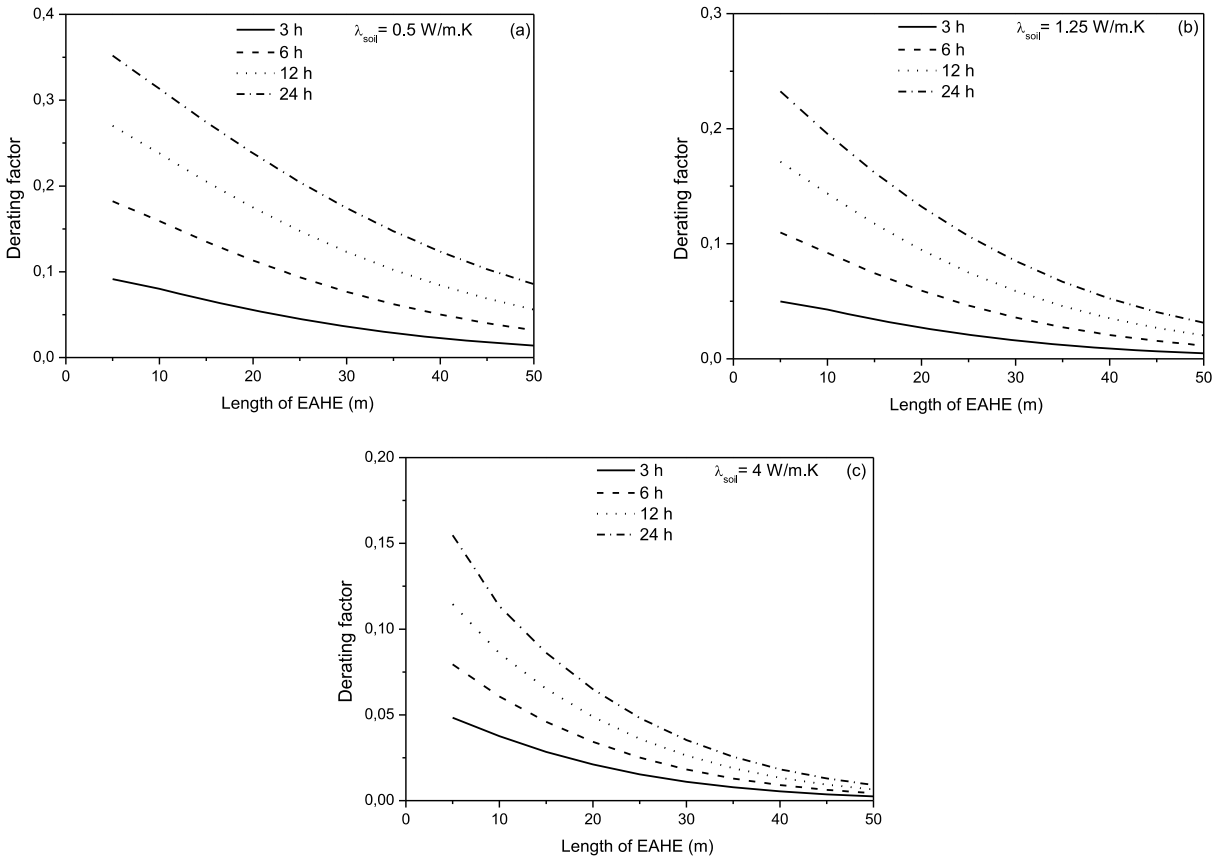

Fig. 10. Transient variation in derating factor along the EAHE for various soil thermal conductivities.

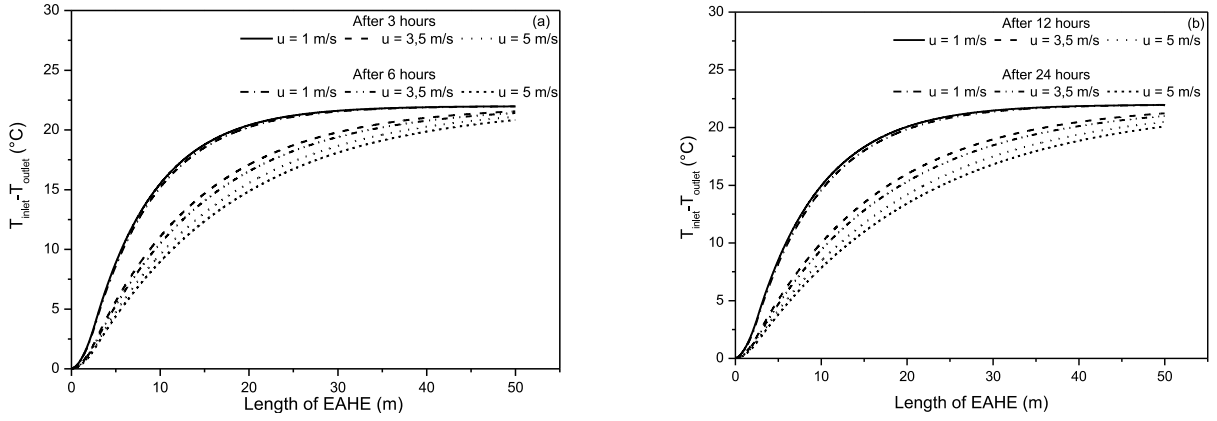

Fig. 11. Transient air temperature drop inside the EAHE for various air flow velocities.

from table 7 under transient and steady state conditions. It is clear that the thermal performance of EAHE is greatly affected in transient operation mode assuming the condition montioned above. From table 7 under steady state condition, it is noted that maximum difference in air temperature is 23.52 °C.

Fig. 8 presents the hourly soil temperature variation in different layers near the pipe along the EAHE during 57 h of continuous operation. 4 rays of the soil are taken into account to show the effect of air temperature on the soil surrounding the pipe. It is noted that the soil temperature represented in Fig. 8 was calculated using Eq. (17) by introducing the experimental data of air temperature in tables 3, 4 and 5. For that the soil temperature at the pipe's inlet (0 m) is supposed to be the same as the inlet air temperature. It is observed that the drops in soil temperature between $2r_1$ and $5r_1$ at 20 m pipe's length is 0.23, 0.14 and 0.20 °C after 9, 37 and 57 h respectively of continuous operation. which means that the radius of the soil r_3 has no effect in the next length of the pipe.

In Fig. 9 (a and b), three different soil thermal conductivities of 0.5, 1.25 and 4 /m.k are considered while assessing thermal performances and determining the soil's ideal thermal conductivity. For soil thermal conductivities of 0.5, 1.25 and 4 W/m.k and a duration of 24 h, it was observed an increase of 1.53, 0.57 and 0.14 °C in air temperatures at the EAHE's outlet respectively. Therefore, low thermal conductivity of the soil has a significant effect on EAHE's thermal performances. The soil's high thermal conductivity allows heat accumulated to be evacuated away from the EAHE.

The curves in Fig. 10 (a, b and c) represent the derating factor of the EAHE's thermal performances. Derating factor is defined as the ratio of

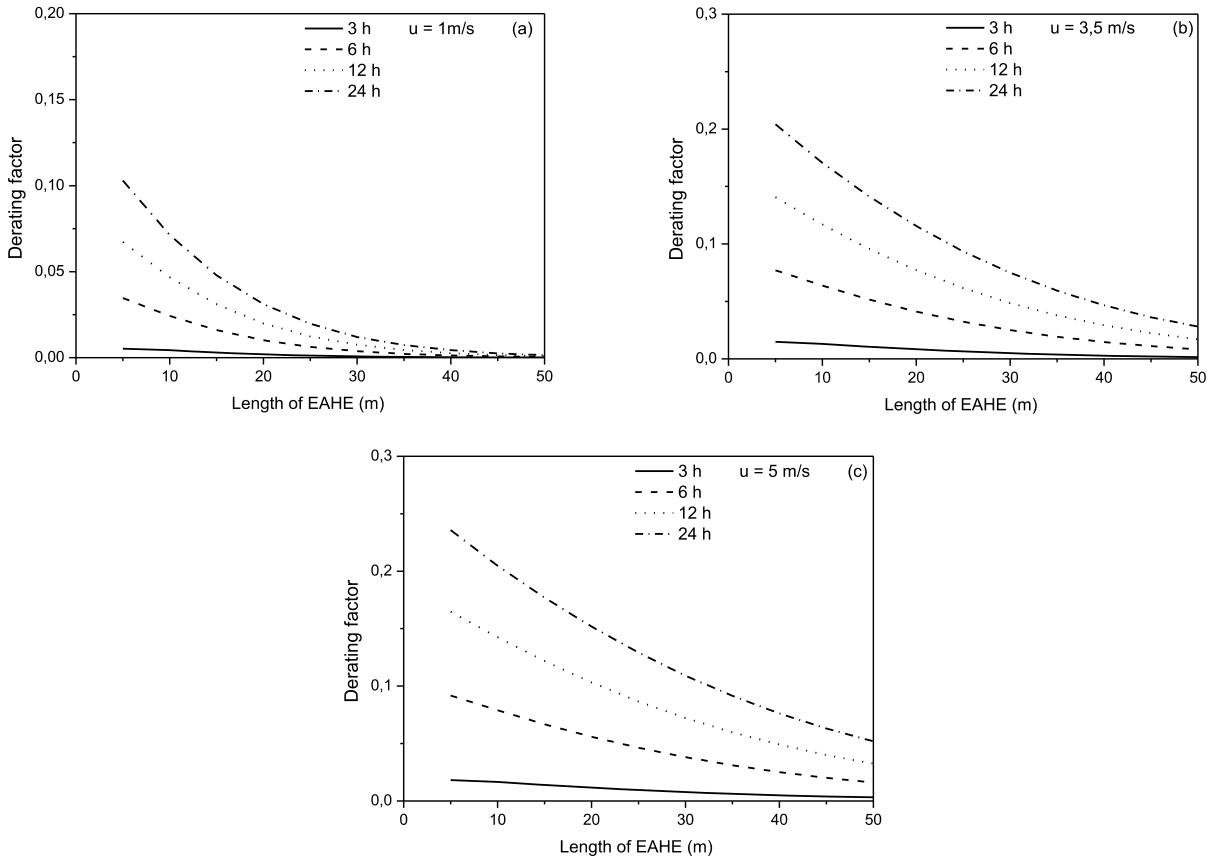

Fig. 12. Transient variation in derating factor along the EAHE for various air flow velocities.

deterioration in thermal performance under transient conditions compared to the thermal performance under steady state conditions. It also demonstrates how the EAHE's thermal performance degrades as a result of the continuous operation mode. To determine the derating factor, temperature drops obtained under steady state and transient conditions are used as shown in Eq. (13).

It is observed that the derating factor increases with duration of operation due to the increase in the outlet air temperature under transient condition. The increase in the outlet air temperature with time is due to the accumulation of heat in the soil surrounding the EAHE, which influences on EAHE's thermal performance and therefore the derating factor increases with time.

When derating factor approaches zero in a section of EAHE, it means that the thermal performance of EAHE in transient condition at that section approaches the thermal performance of EAHE in steady state.

Fig. 11 (a and b) illustrates the transient variation of flowing air temperature inside the EAHE for various air flow velocities (1, 3.5 and 5 m/s). The EAHE's thermal performance is analysed in continuous operation. Air temperature rise as air flow velocity increases, implying that the air does not have enough time to release its heat to the soil. For an operating period of 3 h to 24 h, temperature differences of 1.03, 0.57 and 0.03 °C are observed at the outlet of EAHE for air flow velocities of 5, 3.5 and 1 m/s respectively.

The impact of air flow velocity on EAHE's thermal performances in terms of derating factor is represented in Fig. 12 (a, b and c). The derating factor tends towards zero for all operating times at the EAHE's outlet for low air velocities, taking as example 1 m/s in Fig. 12(a), because of the rapid exchange of heat in the EAHE's few first meters between soil and air. From Fig. 12 (a, b and c), it is clear that thermal performance is affected by increasing the air flow velocity inside the pipe. Therefore, it is not advisable to severely increase the air flow velocity inside the tube.

5. Conclusion

In this paper, the impact of EAHE's continuous operation mode on its thermal performances is discussed. Air temperatures along the EAHE have been numerically determined exploiting a thermal numerical approach based mainly on the energy balances principle in both steady and transient conditions. Besides, an experimental setup was realized at the University of Biskra (Algeria) to examine the effect of EAHE's continuous operation mode on thermal performance in hot and arid climatic conditions. For this reason, experimental measurements were conducted during the summer period from July to September 2013. During the experimental measurements, three different air flow velocities of 2, 3.5 and 4.5 m/s are considered. The air temperatures inside the buried pipe were taken at 15 different locations every 15 min during 95 h.

The study's findings are analysed, and the following conclusions can be inferred:

- EAHE's thermal performances is influenced by high air velocity and low soil thermal conductivity.
- High inlet air temperatures induce heat to accumulate on the soil layers near the EAHE.
- The first 33 m of the EAHE can provide 91% of the overall air temperatures reduction. For this reason, there are no major benefits to adopting EAHE above a 33 m length.
- During continuous operation of EAHE with air flow velocity of 3.5 m/s, the highest increase in air temperature at the pipe's outlet can reach up 0.85 °C and the maximum air temperature drop can reach up 19 °C.
- The outlet air temperatures are unaffected by the continuous operation mode of 95 h due to high soil thermal conductivity.

- The ambient air temperature drops during night-time, cooling the heated sub-soil and assisting the soil in regaining its cooling capacity.

Declaration of Competing Interest

The authors declare that they have no known competing financial interests or personal relationships that could have appeared to influence the work reported in this paper.

Acknowledgments

This study was supported by the Directorate General of Scientific Research and Technological Development (DGRSDT) of the Algerian Ministry of Higher Education and Scientific Research as a part of PRFU project [A11N01UN070120220002].

References

Ahmed, S., Amanullah, M., Khan, M., Rasul, M., Hassan, N., 2016. Parametric study on thermal performance of horizontal earth pipe cooling system in summer. Energy Convers. Manage. 114, 324–337. https://doi.org/10.1016/j.enconman.2016.01.061.

Al-Ajmi, F., Loveday, D.L., Hanby, V.I., 2006. The cooling potential of earth–air heat exchangers for domestic buildings in a desert climate. Build. Environ. 41 (3), 235–244. https://doi.org/10.1016/j.buildenv.2005.01.027.

Bansal, V., Misra, R., Agarwal, G.D., Mathur, J., 2013. Derating Factor' new concept for evaluating thermal performance of earth air tunnel heat exchanger: a transient CFD analysis. Appl. Energy 102, 418–426. https://doi.org/10.1016/j.apenergy.2012.07.027.

Barakat, S., Ramzy, A., Hamed, A.M., El Emam, S.H., 2016. Enhancement of gas turbine power output using earth to air heat exchanger (EAHE) cooling system. Energy Convers. Manage. 111, 137–146. https://doi.org/10.1016/j.enconman.2015.12.060.

Belloufi, Y., 2017. PhD thesis. Université Mohamed Khider-Biskra.

Belloufi, Y., Brima, A., Zerouali, S., Atmani, R., Aissaoui, F., Rouag, A., Moummi, N., 2017. Numerical and experimental investigation on the transient behavior of an earth air heat exchanger in continuous operation mode. Int. J. Heat Technol. 35 (2), 279–288. https://doi.org/10.18280/ijht.350208.

Benhammou, M., Draoui, B., 2015. Parametric study on thermal performance of earth-to-air heat exchanger used for cooling of buildings. Renewable Sustainable Energy Rev. 44, 348–355. https://doi.org/10.1016/j.rser.2014.12.030.

Bozis, D., Papakostas, K., Kyriakis, N., 2011. On the evaluation of design parameters effects on the heat transfer efficiency of energy piles. Energy Build. 43 (4), 1020–1029. https://doi.org/10.1016/j.enbuild.2010.12.028.

Cuny, M., Lin, J., Siroux, M., Fond, C., 2019. Influence of an improved surrounding soil on the energy performance and the design length of earth-air heat exchanger. Appl. Therm. Eng. 162, 114320 https://doi.org/10.1016/j.applthermaleng.2019.114320.

de Jesus Freire, A., Alexandre, J.L.C., Silva, V.B., Couto, N.D., Rouboa, A., 2013. Compact buried pipes system analysis for indoor air conditioning. Appl. Therm. Eng. 51 (1), 1124–1134. https://doi.org/10.1016/j.applthermaleng.2012.09.045.

Diersch, H.J.G., Bauer, D., Heidemann, W., Rühaak, W., Schätzl, P., 2011. Finite element modeling of borehole heat exchanger systems: part 2. Numerical simulation. Comput. Geosci. 37 (8), 1136–1147. https://doi.org/10.1016/j.cageo.2010.08.002.

Fazlikhani, F., Goudarzi, H., Solgi, E., 2017. Numerical analysis of the efficiency of earth to air heat exchange systems in cold and hot-arid climates. Energy Convers. Manage. 148, 78–89. https://doi.org/10.1016/j.enconman.2017.05.069.

Hamdane, S., Mahboub, C., Moummi, A., 2021. Numerical approach to predict the outlet temperature of earth-to-air-heat-exchanger. Thermal Science and Engineering Progress 21. https://doi.org/10.1016/j.tsep.2020.100806.

Hermes, V.F., Ramalho, J.V.A., Rocha, L.A.O., dos Santos, E.D., Marques, W.C., Costi, J., Rodrigues, M.K., Isoldi, L.A., 2020. Further realistic annual simulations of earth-air heat exchangers installations in a coastal city. Sustainable Energy Technologies and Assessments 37, 100603. https://doi.org/10.1016/j.seta.2019.100603.

Hollmuller, P., 2003. Analytical characterisation of amplitude-dampening and phase-shifting in air/soil heat-exchangers. Int. J. Heat Mass Transf. 46 (22), 4303–4317. https://doi.org/10.1016/S0017-9310(03)00199-6.

Jalaluddin, Miyara, A., Tsubaki, K., Inoue, S., Yoshida, K., 2011. Experimental study of several types of ground heat exchanger using a steel pile foundation. Renew Energy 36 (2), 764–771. https://doi.org/10.1016/j.renene.2010.08.011.

Kumar, R., Ramesh, S., Kaushik, S.C., 2003. Performance evaluation and energy conservation potential of earth–air–tunnel system coupled with non-air-conditioned building. Build. Environ. 38 (6), 807–813. https://doi.org/10.1016/S0360-1323(03)00024-6.

Lee, K.H., Strand, R.K., 2008. The cooling and heating potential of an earth tube system in buildings. Energy Build. 40 (4), 486–494. https://doi.org/10.1016/j.enbuild.2007.04.003.

Liu, Z., Sun, P., Xie, M., Zhou, Y., He, Y., Zhang, G., Chen, D., Li, S., Yan, Z., Qin, D., 2021. Multivariant optimization and sensitivity analysis of an experimental vertical earth-to-air heat exchanger system integrating phase change material with Taguchi method. Renew Energy 173, 401–414. https://doi.org/10.1016/j.renene.2021.03.106.

Liu, Z., Yu, Z., Yang, T., Li, S., Mankibi, M.E., Roccamena, L., Qin, D., Zhang, G., 2019a. Designing and evaluating a new earth-to-air heat exchanger system in hot summer and cold winter areas. Energy Procedia 158, 6087–6092. https://doi.org/10.1016/j.egypro.2019.01.506.

Liu, Z., Yu, Z., Yang, T., Roccamena, L., Sun, P., Li, S., Zhang, G., El Mankibi, M., 2019b. Numerical modeling and parametric study of a vertical earth-to-air heat exchanger system. Energy 172, 220–231. https://doi.org/10.1016/j.energy.2019.01.098.

Liu, Z., Yu, Z.J., Yang, T., El Mankibi, M., Roccamena, L., Sun, Y., Sun, P., Li, S., Zhang, G., 2019c. Experimental and numerical study of a vertical earth-to-air heat exchanger system integrated with annular phase change material. Energy Convers. Manage. 186, 433–449. https://doi.org/10.1016/j.enconman.2019.02.069.

Mathur, A., Srivastava, A., Agrawal, G.D., Mathur, S., Mathur, J., 2015a. CFD analysis of EATHE system under transient conditions for intermittent operation. Energy Build. 87, 37–44. https://doi.org/10.1016/j.enbuild.2014.11.022.

Mathur, A., Surana, A.K., Verma, P., Mathur, S., Agrawal, G.D., Mathur, J., 2015b. Investigation of soil thermal saturation and recovery under intermittent and continuous operation of EATHE. Energy Build. 109, 291–303. https://doi.org/10.1016/j.enbuild.2015.10.010.

Mehdid, C.-.E., Benchabane, A., Rouag, A., Moummi, N., Melhegueg, M.-.A., Moummi, A., Benabdi, M.-.L., Brima, A., 2018. Thermal design of Earth-to-air heat exchanger. Part II a new transient semi-analytical model and experimental validation for estimating air temperature. J. Clean Prod. 198, 1536–1544. https://doi.org/10.1016/j.jclepro.2018.07.063.

Menhoudj, S., Mokhtari, A.M., Benzaama, M.-.H., Maalouf, C., Lachi, M., Makhlouf, M., 2018. Study of the energy performance of an earth—Air heat exchanger for refreshing buildings in Algeria. Energy Build. 158, 1602–1612. https://doi.org/10.1016/j.enbuild.2017.11.056.

Mihalakakou, G., 2003. On the heating potential of a single buried pipe using deterministic and intelligent techniques. Renew Energy 28 (6), 917–927. https://doi.org/10.1016/S0960-1481(02)00183-0.

Minaei, A., Talee, Z., Safikhani, H., Ghaebi, H., 2021. Thermal resistance capacity model for transient simulation of Earth-Air Heat Exchangers. Renew Energy 167, 558–567. https://doi.org/10.1016/j.renene.2020.11.114.

Misra, R., Bansal, V., Agrawal, G.D., Mathur, J., Aseri, T., 2013a. Transient analysis based determination of derating factor for earth air tunnel heat exchanger in summer. Energy Build. 58, 103–110. https://doi.org/10.1016/j.enbuild.2012.11.001.

Misra, R., Bansal, V., Agrawal, G.D., Mathur, J., Aseri, T.K., 2013b. CFD analysis based parametric study of derating factor for Earth Air Tunnel Heat Exchanger. Appl. Energy 103, 266–277. https://doi.org/10.1016/j.apenergy.2012.09.041.

Mnasri, T., Younès, R.B., 2010. Modeling of Unsteady Turbulent Flow in a Buried Co-Axial Exchanger—The Use of Green's Functions Theory. Numerical Heat Transfer, Part A: Applications 58 (12), 963–983. https://doi.org/10.1080/10407782.2010.529031.

Niu, F., Yu, Y., Yu, D., Li, H., 2015. Heat and mass transfer performance analysis and cooling capacity prediction of earth to air heat exchanger. Appl. Energy 137, 211–221. https://doi.org/10.1016/j.apenergy.2014.10.008.

Nougier, J.P., 1987. Méthodes De Calcul Numérique. Masson.

Philippe, M., Bernier, M., Marchio, D., 2009. Validity ranges of three analytical solutions to heat transfer in the vicinity of single boreholes. Geothermics 38 (4), 407–413. https://doi.org/10.1016/j.geothermics.2009.07.002.

Rodrigues, M.K., da Silva Brum, R., Vaz, J., Rocha, L.A.O., dos Santos, E.D., Isoldi, L.A., 2015. Numerical investigation about the improvement of the thermal potential of an Earth-Air Heat Exchanger (EAHE) employing the Constructal Design method. Renew Energy 80, 538–551. https://doi.org/10.1016/j.renene.2015.02.041.

Rosa, N., Santos, P., Costa, J., Gervásio, H., 2018. Modelling and performance analysis of an earth-to-air heat exchanger in a pilot installation. J. Building Phys. 42 (3), 259–287. https://doi.org/10.1177/1744259117754298.

Rouag, A., Benchabane, A., Mehdid, C.-.E., 2018. Thermal design of Earth-to-Air Heat Exchanger. Part I a new transient semi-analytical model for determining soil temperature. J Clean Prod 182, 538–544. https://doi.org/10.1016/j.jclepro.2018.02.089.

Śliwa, T., Kruszewski, M., Zare, A., Assadi, M., Sapińska-Śliwa, A., 2018. Potential application of vacuum insulated tubing for deep borehole heat exchangers. Geothermics 75, 58–67. https://doi.org/10.1016/j.geothermics.2018.04.001.

Wei, H., Yang, D., 2019. Performance evaluation of flat rectangular earth-to-air heat exchangers in harmonically fluctuating thermal environments. Appl. Therm. Eng. 162, 114262 https://doi.org/10.1016/j.applthermaleng.2019.114262.

Wei, H., Yang, D., Du, J., Guo, X., 2021. Field experiments on the effects of an earth-to-air heat exchanger on the indoor thermal environment in summer and winter for a typical hot-summer and cold-winter region. Renew Energy 167, 530–541. https://doi.org/10.1016/j.renene.2020.11.112.

Wei, H., Yang, D., Wang, J., Du, J., 2020. Field experiments on the cooling capability of earth-to-air heat exchangers in hot and humid climate. Appl. Energy 276, 115493. https://doi.org/10.1016/j.apenergy.2020.115493.

Xi, J., Li, Y., Liu, M., Wang, R.Z., 2017. Study on the thermal effect of the ground heat exchanger of GSHP in the eastern China area. Energy 141, 56–65. https://doi.org/10.1016/j.energy.2017.09.060.

Yang, D., Guo, Y., Zhang, J., 2016. Evaluation of the thermal performance of an earth-to-air heat exchanger (EAHE) in a harmonic thermal environment. Energy Convers. Manage. 109, 184–194. https://doi.org/10.1016/j.enconman.2015.11.050.

Yang, D., Zhang, J., 2015. Analysis and experiments on the periodically fluctuating air temperature in a building with earth-air tube ventilation. Build. Environ. 85, 29–39. https://doi.org/10.1016/j.buildenv.2014.11.019.

Zajch, A., Gough, W.A., 2021. Seasonal sensitivity to atmospheric and ground surface temperature changes of an open earth-air heat exchanger in Canadian climates. Geothermics 89, 101914. https://doi.org/10.1016/j.geothermics.2020.101914.
Zhelykh, V., Savchenko, O., Matusevych, V., 2016. Improving efficiency of heat exchange of horizontal ground-air heat exchanger for geothermal ventilation systems. Fizyka budowli w teorii i praktyce 8.
Zhou, S., Cui, W., Tao, J., Peng, Q., 2016. Study on ground temperature response of multilayer stratums under operation of ground-source heat pump. Appl. Therm. Eng. 101, 173–182. https://doi.org/10.1016/j.applthermaleng.2016.02.130.